Journal of the Mechanics and Physics of Solids 136 (2020) 103720

Contents lists available at ScienceDirect

Journal of the Mechanics and Physics of Solids

journal homepage: www.elsevier.com/locate/jmps

Localization in spherical shell buckling

Basile Audoly[a,*], John W. Hutchinson[b]

[a] Laboratoire de mécanique des solides, CNRS, Institut Polytechnique de Paris, France
[b] School of Engineering and Applied Sciences, Harvard University, Cambridge, MA 02138, USA

ARTICLE INFO

Article history:
Received 29 June 2019
Revised 9 September 2019
Accepted 9 September 2019
Available online 12 September 2019

Keywords:
Buckling
Shells and membranes
Stability and bifurcation
Asymptotic analysis

ABSTRACT

This paper addresses localization of the deformation due to buckling that occurs immediately following the onset of bifurcation in the axisymmetric buckling of a perfect spherical elastic shell subject to external pressure. The localization process is so abrupt that the buckling mode of the classical eigenvalue analysis, which undulates over the entire shell, becomes modified immediately after bifurcation transitioning to an isolated dimple surrounded by an unbuckled expanse of the shell. The paper begins by revisiting earlier attempts to analyze the initial post-buckling behavior of the spherical shell, illustrating their severely limited range of validity. The unsuccessful attempts are followed by an approximate Rayleigh-Ritz solution which captures the essence of the localization process. The approximate solution reveals the pathway that begins at bifurcation from the classical mode shape to the localized dimple buckle. The second part of the paper presents an exact asymptotic expansion of the initial post-buckling behavior which accounts for localization and which further exposes the analytic details of the abruptness of the transition.

1. Introduction

Mechanical localization phenomena are more common than is generally appreciated. Necking in a long bar or rod subject to tensile stretching is perhaps the best known example. Prior to the onset of necking relatively uniform straining occurs along the entire length of the bar, but once necking sets in the additional deformation localizes in the neck which typically has a length on the order of the bar diameter. Pipes, tubes and straws subject to overall bending distribute the curvature along their length until suddenly the additional curvature changes localize at one section whose length is again on the order of the diameter of the member. This paper addresses buckling localization in shells, specifically in elastic spherical shells subject to external pressure. Our primary aim is to expose the abrupt transition from a buckling mode that is distributed over the entire shell at the onset of buckling to a buckling mode that is a localized dimple in a small region of the shell and unbuckled outside that region.

There are two features common to nearly all mechanical localization phenomena: a competition between two well separated deformation scales, an overall scale and a local scale, and a diminishing load carrying capacity attained at some stage with increasing deformation at the overall scale. For necking of the long tensile bar, the two scales are the length and the diameter of the bar. The second feature is met for most metals and some polymers because a bar of these materials displays a maximum load followed by decreasing load under uniaxial tension. For long cylindrical shells undergoing elastic bending, the two scales are again the length and the diameter. These structural entities display a maximum moment in

* Corresponding author.
E-mail address: audoly@lmm.jussieu.fr (B. Audoly).

https://doi.org/10.1016/j.jmps.2019.103720
0022-5096/

overall bending followed by decreasing moment, either due to cross-sectional ovalization or to a short wavelength buckling mode on the compressive side of the shell. In spherical shell buckling of interest here, the two scales are the characteristic wavelength of the buckling mode, which is on the order of $\sqrt{Rt}$ with R as the shell radius and t as its thickness, and the size of the shell itself, of order R. The second feature making spherical shell buckling susceptible to localization is the drop in pressure carrying capacity which coincides with the onset of buckling. In each of these cases, a physical argument applies analogous to that put forward by Considère (1885) to explain necking localization in a long bar stretched in tension. Namely, a slight imperfection somewhere along the bar causes the maximum load to be attained at that location and, then, with continuing deformation at that location, the load falls at the other locations along the bar because the maximum load is never reached in those locations. Outside the neck the bar unloads. Tvergaard and Needleman (1980) have interpreted the corresponding scenario for bending localization in cylindrical tubes and shells along the lines laid out by Considère, while the book by Kyriakides and Corona (2007) reports both numerical studies and an extensive series of experiments on bending localization in pipelines.

The importance of localization in the elastic buckling of cylindrical shells subject to axial compression has recently emerged in the published work of Horák et al. (2006), Kreilos and Schneider (2017) and Groh and Pirrera (2019). Localization in cylindrical shells has features in common with that in the spherical shell, however, cylindrical shell buckling is inherently two dimensional involving variations in both the axial and circumferential directions. As a consequence the behavior of the cylinder is governed by partial differential equations and the analyses noted above have been numerical. For the perfect elastic cylindrical shell under axial compression, stable localized dimple-like buckles have been shown to exist at loads above those the shell can support for more widely distributed buckle patterns suggesting that cylindrical shells with a sufficiently low level of imperfection may be capable of carrying higher loads that the design codes currently allow. An attractive feature of spherical shells is that an important set of buckling localizations can be studied for shells undergoing axisymmetric deformation such that the behavior is governed by ordinary, not partial, differential equations. This, in turn, increases the possibility of obtaining insight from analytical solution methods of various kinds, as well enabling simpler numerical methods. In this paper we will exploit both analytical and numerical methods to expose the nature of localization in the elastic buckling of a perfect spherical shell subject to uniform external pressure.

1.1. Background preliminaries to localization in spherical shells

As background to the present study, we begin by citing basic results for the classical elastic buckling of a thin, perfect spherical shell subject to external pressure. The axisymmetric response of the spherical shell fully captures the localization phenomena of interest here, and throughout this paper attention will be restricted to axisymmetric behavior. Let β be the meridian angle measured from the upper pole of the shell. With $\overline{p}$ as the external pressure acting on the shell and $\overline{w}(\beta)$ as the outward normal deflection of the shell middle surface, the classical buckling, or bifurcation, pressure and the associated buckling eigenmode are

$$\overline{p}_{\rm c} = \frac{2Et^2}{\sqrt{3(1-\nu^2)}R^2} \qquad \text{and} \qquad \overline{w}_1(\beta) \propto P_n(\cos\beta). \tag{1.1}$$

Here, E is Young's modulus and ν is Poisson's ratio, $P_n(x)$ is the Legendre polynomial of degree n, and n is the integer most closely satisfying $n(n+1) = \sqrt{12(1-\nu^2)}\frac{R}{t}$. The magnitude of the classical buckling mode is largest at the poles but the mode extends over the entire shell with a wavelength proportional to $\sqrt{Rt}$. A collage of some of the details of the localization process in the buckling of an elastic spherical shell under external pressure is presented in Fig. 1. These results have been computed in the same manner employed in Hutchinson (2016) using an accurate numerical algorithm for solving nonlinear ordinary differential equations. The normal buckling displacement is defined throughout as $\Delta\overline{w}(\beta) = \overline{w}(\beta) - \overline{w}_0$ where $\overline{w}_0$ is the uniform displacement of the unbuckled shell due to $\overline{p}$:

$$\overline{w}_0 = -\frac{(1-\nu)\overline{p}R^2}{2Et}. \tag{1.2}$$

The buckling displacement at the pole δ is defined positive inward such that $\delta = -\Delta\overline{w}(0)$.

The plot in Fig. 1(b) shows the drop in the pressure as the shell buckles, and this dimensionless curve becomes independent of R/t and ν after localization has set in for thin shells with $R/t > 50$. The classical mode is evident in the buckling deflection in the top middle plot with undulations spread over the entire shell but already at this very small buckling deflection localization has begun, as will emerge more clearly in the sequel. When the pressure has dropped to about $p/p_{\rm c} = 0.9$ and the pole buckling deflection is about 0.3 times the shell thickness, buckling is fully localized in the form of a dimple at the pole, as seen in the bottom middle plot. Not only is localization fully established long before the dimple at the pole has 'inverted', which occurs at $\delta \approx 10t$ (Hutchinson and Thompson, 2017), but it is even fully established well before the local curvature at the pole becomes flat, which occurs when $\delta \approx t$. Asymptotic formulas valid for deflections greater than about one shell thickness have been derived by Evkin et al. (2016) for dimple buckling. Very recently, Baumgarten and Kierfeld (2019) have also obtained a complete set of asymptotic results in the weakly post-buckled regime where localization is present, i.e., up to $\delta \approx t/10$. Their approach allows them to obtain directly the deflection at the pole without calculating the solution in the full domain, and they do not address localization per se. The realization that localized dimple buckles existed in spherical shells without an understanding of how they relate to the classical buckling mode dates back to

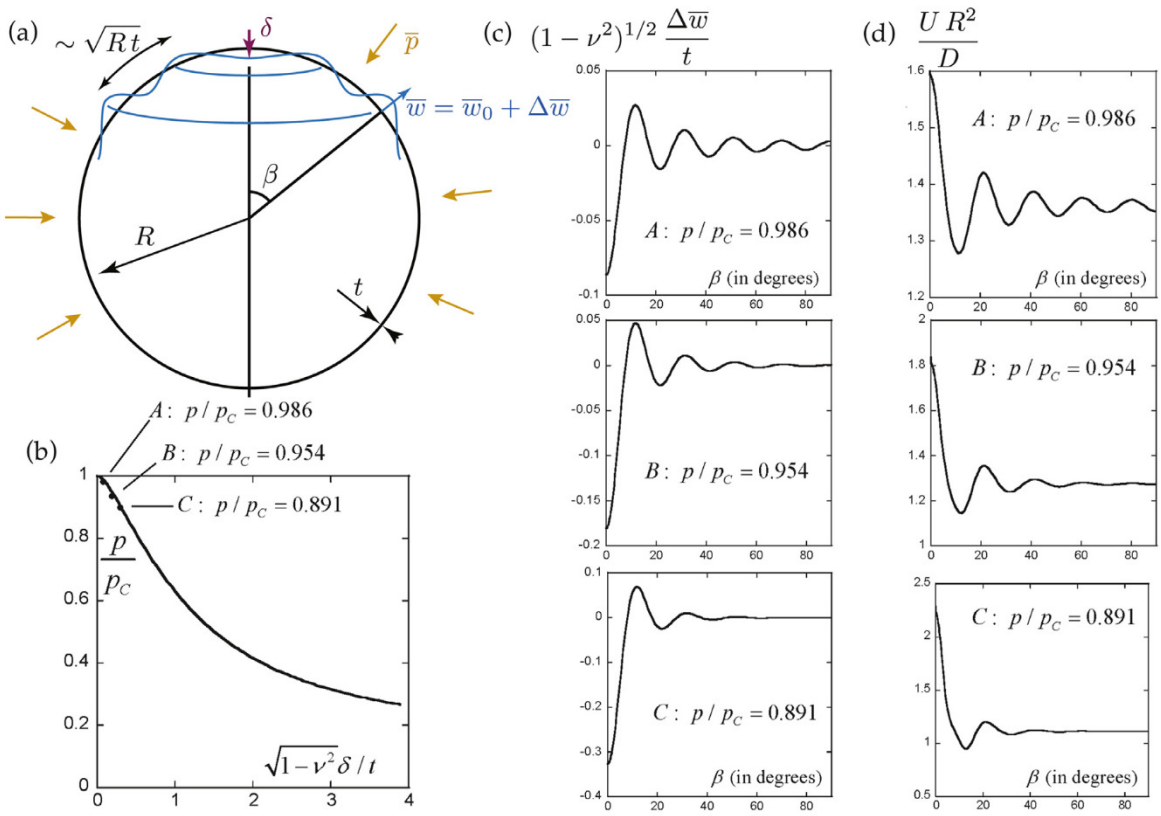

Fig. 1. The progression of buckling localization in a perfect full spherical shell undergoing axisymmetric deformation that is symmetric with respect to equator. (a) Geometry of the spherical shell. (b) Normalized pressure, p/p_c, versus the dimensionless buckling deflection at the pole, $\sqrt{1-\nu^2}\delta/t$. (c) Dimensionless normal buckling displacement, $\sqrt{1-\nu^2}\Delta\overline{w}/t$, as a function of β at three values of p/p_c labeled A, B and C immediately following the onset of buckling. (d) Distribution of the dimensionless elastic strain energy/area, UR^2/D, at the same three values of p/p_c. These dimensionless results have been computed numerically for a shell with $R/t = 103.5$ and $\nu = 0.3$ ($n = 18$), however the dimensionless results for p/p_c versus $\sqrt{1-\nu^2}\delta/t$ become independent of R/t and ν after localization occurs.

some of the earliest studies with von Kármán and Tsien (1939) citing experimental observations, the numerical solutions for buckled deep spherical caps of Bushnell (1965), and the early numerical axisymmetric solutions for full spherical shells of Bauer et al. (1970).

The abruptness of this localization process will be investigated here. This study will shed light on the difficulty encountered by earlier attempts such as those of Thompson (1964) and Koiter (1969) to analyze the post-buckling behavior of the spherical shell using expansion methods that employ the classical buckling mode as the dominant contribution to the deflection. Included in Fig. 1(d) are plots of the distribution of the strain energy per area U in the shell at the same three post-buckling states in dimensionless form UR^2/D where $D = Et^3/[12(1-\nu^2)]$ is the bending stiffness. Immediately following bifurcation undulations reflecting the classical mode are evident, but as localization progresses the energy density becomes uniformly distributed away from the pole and equal to that of the uniform unbuckled solution.

The organization of the paper is as follows. The equations employed to model the shell are listed at the end of this introduction. Results of two initial post-buckling expansions of the type promulgated by Koiter (1945, 1969) are presented in Section 2. These highlight the limited range of validity of the Koiter expansions for spherical shell buckling. An approximate Rayleigh-Ritz solution which captures localization is presented in Section 3 providing an approximate solution with a much larger range of validity. The last section of the paper present an exact (asymptotic) expansion which reveals analytically the progression of the localization process immediately following the onset of buckling.

1.2. The shallow shell model

Analytically it is easier to deal with the equations of *shallow shell theory* for the spherical shell as opposed to the equations of moderate rotation theory for the full shell. Moreover, the essential features of buckling localization for the spherical shell under external pressure are fully revealed by shallow shell theory for spherical caps with sufficient height because continuing deformation localizes to the vicinity of the pole. This is the model which will be analyzed in this paper. Once localization occurs the solution predicted using shallow shell theory coincides to high accuracy with that of moderate

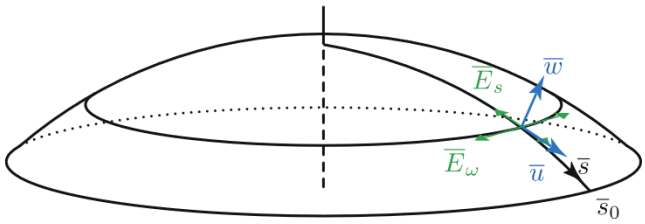

Fig. 2. Geometry of a shallow shell.

rotation theory for the full spherical shell (Hutchinson and Thompson, 2017). The range of pressures for which the shallow shell and the full shell models agree will be specified in the discussion (Section 5).

Let $\overline{s}$ be the meridional distance along the middle surface of the spherical cap and let $\overline{u}(\overline{s})$ and $\overline{w}(\overline{s})$ be the tangential and outward normal displacements of the middle surface, as sketched in Fig. 2. The stretching and bending strains in shallow shell theory for a perfect spherical cap deforming axisymmetrically are

$$\overline{E}_\theta = \frac{\mathrm{d}\overline{u}}{\mathrm{d}\overline{s}} + \frac{\overline{w}}{R} + \frac{1}{2}\left(\frac{\mathrm{d}\overline{w}}{\mathrm{d}\overline{s}}\right)^2 \tag{1.3}$$

$$\overline{E}_\omega = \frac{\overline{u}}{\overline{s}} + \frac{\overline{w}}{R} \tag{1.4}$$

$$\overline{K}_\theta = -\frac{\mathrm{d}^2\overline{w}}{\mathrm{d}\overline{s}^2} \tag{1.5}$$

$$\overline{K}_\omega = -\frac{1}{\overline{s}}\frac{\mathrm{d}\overline{w}}{\mathrm{d}\overline{s}}. \tag{1.6}$$

The work conjugate resultant in-plane stresses and bending moments are

$$\begin{aligned}(\overline{N}_\theta, \overline{N}_w) &= \frac{Et}{1-\nu^2}(\overline{E}_\theta + \nu\overline{E}_\omega, \overline{E}_\omega + \nu\overline{E}_\theta)\\ (\overline{M}_\theta, \overline{M}_w) &= D(\overline{K}_\theta + \nu\overline{K}_\omega, \overline{K}_\omega + \nu\overline{K}_\theta).\end{aligned} \tag{1.7}$$

The principle of virtual work (with $\overline{p}$ positive inward) is

$$\int_0^{\overline{s}_0} \{\overline{M}_\theta\delta\overline{K}_\theta + \overline{M}_\omega\delta\overline{K}_\omega + \overline{N}_\theta\delta\overline{E}_\theta + \overline{N}_\omega\delta\overline{E}_\omega + \overline{p}\delta\overline{w}\}\overline{s}\mathrm{d}\overline{s} = 0, \tag{1.8}$$

where $\overline{s}_0$ is the distance from the pole to the edge of the shell. The boundary conditions introduced below produce no work on the shell edge.

1.3. Dimensionless shallow shell equations

The dimensionless forms of these equations used in the analysis make use of scaled variables that are denoted without an over-bar,

$$\begin{aligned}s &= \frac{(12(1-\nu^2))^{1/4}}{\sqrt{Rt}}\overline{s}\\ w &= \frac{(12(1-\nu^2))^{1/2}}{t}\overline{w}\\ u &= \frac{(12(1-\nu^2))^{3/4}}{(1+\nu)t}\sqrt{\frac{R}{t}}\overline{u}\\ (E_\theta, E_w) &= (12(1-\nu^2))^{1/2}\frac{R}{t}(\overline{E}_\theta, \overline{E}_w)\\ (K_\theta, K_w) &= R(\overline{K}_\theta, \overline{K}_w)\\ (N_\theta, N_w) &= (12(1-\nu^2))^{1/2}\frac{R}{Et^2}(\overline{N}_\theta, \overline{N}_w)\\ (M_\theta, M_w) &= 12(1-\nu^2)\frac{R}{Et^3}(\overline{M}_\theta, \overline{M}_w)\\ p &= (12(1-\nu^2))^{1/2}\frac{R^2}{Et^2}\overline{p}\end{aligned} \tag{1.9}$$

We consider a *thin* shell, in the sense that the wavelength $\sim\sqrt{Rt}$ of the initial buckling mode is much smaller than the shell's dimension $\bar{s}_0$: $\bar{s}_0 \gg \sqrt{Rt}$. This implies that the scaled radius is a large number,

$$s_0 \gg 1. \tag{1.10}$$

The existence of a large number in the problem is at the heart of the asymptotic method capturing the onset of localization, as presented in Section 4.

In terms of the scaled variables, the stretching and bending strains write

$$\begin{aligned} E_\theta &= (1+\nu)u' + w + \frac{1}{2}w'^2 \\ E_\omega &= (1+\nu)\frac{u}{s} + w \\ K_\theta &= -w'' \\ K_\omega &= -\frac{w'}{s}, \end{aligned} \tag{1.11}$$

with primes denoting differentiation with respect to the scaled arc-length, $(\cdot)' = \mathrm{d}(\cdot)/\mathrm{d}s$. The constitutive law take the scaled form

$$\begin{aligned} (N_\theta, N_w) &= \frac{1}{1-\nu^2}(E_\theta + \nu E_\omega, E_\omega + \nu E_\theta) \\ (M_\theta, M_w) &= (K_\theta + \nu K_\omega, K_\omega + \nu K_\theta), \end{aligned} \tag{1.12}$$

and the principle of virtual work becomes

$$\int_0^{s_0} \{M_\theta \delta K_\theta + M_\omega \delta K_\omega + N_\theta \delta E_\theta + N_\omega \delta E_\omega + p\delta w\} s\mathrm{d}s = 0. \tag{1.13}$$

With this choice of variables, the only parameters are s_0 and ν plus the dimensionless pressure p.

The equilibrium equations generated by (1.13) are

$$\frac{1}{s}(sM_\theta)'' - \frac{1}{s}M_\omega' - (N_\theta + N_\omega) + \frac{1}{s}(sN_\theta w')' - p = 0 \tag{1.14a}$$

$$(sN_\theta)' - N_\omega = 0. \tag{1.14b}$$

The boundary conditions for the spherical cap require that the solution is well behaved at the pole. At both the pole ($s = 0$) and the edge ($s = s_0$) the displacements satisfy

$$u = 0 \qquad w' = 0 \qquad \left(\frac{1}{s}(sw')'\right)' = 0, \tag{1.15}$$

where the last condition follows from $(sM_\theta)' - M_\omega = 0$ which ensures there is no concentrated force at the pole and no force per unit edge length. The uniform solution of the unbuckled shell (u_0, w_0) satisfies the field equations and these boundary conditions with $u_0(s) = 0$ and $w_0(s)$ given by (1.2).

The in-plane equilibrium Eq. (1.14b) is automatically satisfied by stresses generated by a stress function, $f(s)$, with

$$N_\theta = \frac{1}{s}f \qquad N_\omega = f'. \tag{1.16}$$

Compatibility of the in-plane strains requires

$$\left(\frac{1}{s}(sf)'\right)' = w' - \frac{1}{s}\frac{w'^2}{2}. \tag{1.17}$$

2. Koiter's initial post-buckling expansions

In this section, we present Koiter's initial post-buckling expansion, both in the standard and extended forms, for the shell model presented in Section 1.3, namely shallow spherical shells under external pressure undergoing axisymmetric deformations. Note that a translation of the Koiter's disseration is available in English (Riks, 1970).

2.1. Elimination of tangent displacement

In dimensionless form, the uniform, unbuckled solution for a perfect shell with the boundary conditions specified in (1.15) is

$$w_0(s) = -(1-\nu)\frac{p}{2} \qquad u_0(s) = 0 \qquad f_0(s) = -\frac{ps}{2}. \tag{2.1}$$

Denote a buckled solution by

$$w(s) = w_0(s) + \tilde{w}(s) \qquad u(s) = u_0(s) + \tilde{u}(s) \qquad f(s) = f_0(s) + \tilde{f}(s) \tag{2.2}$$

The form of the system energy given next, which is expressed in terms of $\tilde{w}$ alone, is particularly useful in carrying out the Koiter expansions and the approximate localization analysis to follow. In the Supplementary Materials, we show that the change in energy of the system from the uniform unbuckled state at prescribed p can be expressed as

$$\Phi(\tilde{w}, p) = \int_0^{s_0} \left\{ \frac{1}{2}\left((\nabla^2\tilde{w})^2 + \tilde{w}^2 - \frac{p}{2}\tilde{w}'^2 \right) + \tilde{w} G_2(\tilde{w}, s) + \frac{1}{2}[G_2(\tilde{w}, s)]^2 \right\} s\mathrm{d}s \tag{2.3}$$

where $G_2(\tilde{w}, s) = \int_s^{s_0} (2x)^{-1}\tilde{w}'^2(x)\mathrm{d}x$ and $\nabla^2\tilde{w} = s^{-1}(s\tilde{w}')'$ as the Laplacian associated with the metric $\int \cdot s\mathrm{d}s$. The energy change comprises contributions that are quadratic, cubic and quartic in $\tilde{w}$. Contributions that depend on Poisson's ratio have either been absorbed into the dimensionless quantities or integrated to zero for the boundary condition under consideration. With p as the prescribed pressure, the only parameter in the energy functional is s_0. The geometric boundary conditions on $\tilde{w}$ require that $\tilde{w}' = 0$ at $s = 0$ and $s = s_0$. These are coupled with the natural boundary conditions requiring $(s^{-1}(s\tilde{w}')')' = 0$ at ends of the interval, see Eq. (1.15).

The stress function $\tilde{f}$, which is now auxiliary, is given in terms of $\tilde{w}$ by

$$\tilde{f}(s) = -\frac{1}{s}\int_s^{s_0} (\tilde{w}(x) + G_2(\tilde{w}, x))x\mathrm{d}x \tag{2.4}$$

The Euler equation characterizing the buckled states is generated by $\delta\Phi = 0$ for all admissible $\delta\tilde{w}$ and is given by

$$\nabla^4\tilde{w} + \tilde{w} + \frac{p}{2}\nabla^2\tilde{w} = -G_2(\tilde{w}, s) + \frac{1}{s}(\tilde{f}\tilde{w}')'. \tag{2.5}$$

where $\nabla^4\tilde{w} = \nabla^2(\nabla^2\tilde{w})$ and $\tilde{f}$ is given in terms of $\tilde{w}$ by (2.4).

2.2. The classical buckling mode and pressure

The differential equation for the eigenvalue problem governing the classical buckle problem is given by (2.5) linearized with respect to $\tilde{w}$:

$$\nabla^4 w_1 + w_1 + \frac{p}{2}\nabla^2 w_1 = 0 \quad \text{with } w_1' = (s^{-1}(sw_1')')' = 0 \text{ for } s = 0, s_0. \tag{2.6}$$

The eigenmodes have the form $w_1(s) = -J_0(\mu s)$ where μ is any root of $J_1(\mu s_0) = 0$, with J_0 and J_1 as Bessel functions of zeroth and first order. The eigenvalue associated with μ is $p = 2(\mu^2 + \mu^{-2})$. For $r \geq 0$, denote the i^{th} zero of $J_1(r) = 0$, ordered in increasing magnitude, by r_i, $i = 0, \ldots, \infty$ (including $\mu_0 = 0$ as the first root). One sees immediately, that for any s_0 equal to one of these positive roots, say $s_0 = r_N$, the minimum eigenvalue, i.e., the classical buckling pressure p_c, is given by

$$p_c = 4 \tag{2.7}$$

with $\mu_N = 1$. The buckling mode is the eigenmode, $w_1(s) = -J_0(s)$, and the associated stress function is $f_1(s) = -J_1(s)$. Values of s_0 that are not equal to one of the roots r_i will have a higher minimum eigenvalue, but for the shells of interest in this study, the dimensionless base radius s_0 is large, see Eq. (1.10) so that the dimensionless classical buckling pressure is always either 4 or just slightly above.

Without any loss in physical insight, we will focus attention in Sections 2 and 3 on shells with base radius equal to one of the roots, $s_0 = r_N$, where N is large compared to 1.

2.3. Koiter's initial post-buckling expansion

Koiter's 'standard' method develops an expansion about the bifurcation point in the form

$$\tilde{w}(s) = \xi w_1(s) + \xi^2 w_2(s) + \xi^3 w_3(s) + \cdots \qquad \frac{p}{p_c} = 1 + a\xi + b\xi^2 + \cdots, \tag{2.8}$$

with the auxiliary expansion, $\tilde{f}(s) = \xi f_1(s) + \xi^2 f_2(s) + \xi^3 f_3(s) + \cdots$ For the standard expansion it is necessary to specify an orthogonality condition on the higher order contributions, w_j, for the expansion to be unique. Here we require $\int_0^{s_0} w_1 w_j s\mathrm{d}s = 0$ for $j \geq 2$.

The boundary value problem for w_2 obtained from the expansion of (2.5) is

$$\nabla^4 w_2 + w_2 + \frac{p_c}{2}\nabla^2 w_2 = -\frac{p_c}{2}a\nabla^2 w_1 + q_2(s) \tag{2.9}$$

with $q_2(s) = s^{-1}(f_1 w_1')' - G_2(w_1, s)$. The homogeneous boundary conditions listed earlier apply. The solution to the second order problem is constructed using the complete set of eigenfunctions generated by the problem for $v(s)$ on $0 \leq s \leq s_0$: $\nabla^2 v + \mu^2 v = 0$, with v analytic at $s = 0$ with $v'(0) = 0$ and $v'(s_0) = 0$. The eigenfunctions are

$$v_i(s) = J_0(\mu_i s),$$

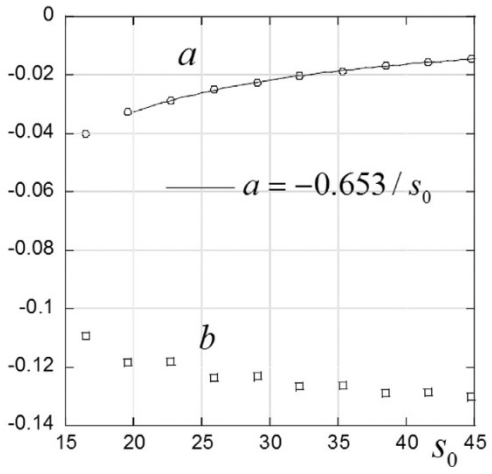

Fig. 3. Plot of the initial post-buckling coefficients for values of $s_0 = r_N$, $5 \le N \le 15$, as predicted by Koiter's standard method, computed with $M = 40$. As $N \to \infty$, $a \to 0$ ($a = -0.653/s_0$ is a fit to the computed values) and $b \to \approx -0.132$.

where μ_i are the eigenvalues satisfying $J_1(\mu_i s_0) = 0$ for $i = 0, \ldots, \infty$. With $s_0 = r_N$, we have $\mu_i = r_i/r_N$ and $\mu_N = 1$. Further, it is easily shown that each eigenfunction satisfies all four boundary conditions required for $\bar{w}$. We expand $q_2(s)$ on the eigenfunctions

$$q_2(s) = \sum_{i=0}^{M} q_2^{(i)} v_i(s) \qquad \text{with } q_2^{(i)} = \int_0^{s_0} q_2(s) v_i(s) s \mathrm{d}s,$$

where the number M of terms retained in the expansion must be sufficient to ensure accuracy, $M \gg 1$.

The existence of a solution to (2.9) requires that the secular term proportional to w_1 on the right hand side of the equation be suppressed, which provides a as

$$a = \frac{q_2^{(N)}}{2}. \tag{2.10}$$

Then

$$w_2(s) = \sum_{j=0}^{M} w_2^{(j)} v_j(s) \tag{2.11a}$$

with

$$w_2^{(0)} = q_2^{(0)} \quad w_2^{(N)} = 0 \quad w_2^{(i)} = \frac{1}{\left(\mu_i^4 + 1 - p_c \mu_i^2\right)} q_2^{(i)}, \quad i \ge 1 (\ne N). \tag{2.11b}$$

Koiter's 'standard' method (see Supplementary Material) provides the following formulas for the initial post-bifurcation expansion coefficients, a and b:

$$\begin{aligned} a &= \frac{3 \int_0^{s_0} G_2(w_1, s) w_1 \, s \mathrm{d}s}{\frac{p_c}{2} \int_0^{s_0} w_1'^2 s \mathrm{d}s} \\ b &= \frac{2 \int_0^{s_0} \left\{ w_1 \int_s^{s_0} x^{-1} w_1' w_2' \mathrm{d}x + (w_2 + G_2(w_1, s)) G_2(w_1, s) \right\} s \mathrm{d}s}{\frac{p_c}{2} \int_0^{s_0} w_1'^2 s \mathrm{d}s} \end{aligned} \tag{2.12}$$

Note that a only depends on w_1. For the present shell problem, one can show by direct manipulation that the expression for a in (2.10) is the same as that in (2.12), and, further, that both can be re-expressed as

$$a = \frac{3 \int_0^{s_0} w_1'^3 \mathrm{d}s}{p_c \int_0^{s_0} w_1'^2 s \mathrm{d}s}. \tag{2.13}$$

Plots of a and b as dependent on N with $s_0 = r_N$ are presented in Fig. 3. Nearly all the integrals such as those in (2.12) and (2.13) have been evaluated numerically in this paper using highly accurate integration algorithms in the IMSL codes (Visual Numerics, 1994). It is worth mentioning that a great deal of Koiter's 1969 paper is taken up with reducing integrals analogous to these so they could be integrated analytically.

While Thompson (1964) and Koiter (1969) analyzed a full spherical shell and the present paper analyzes a spherical cap, the trends in the post-buckling coefficients for the two cases are very similar. In Fig. 3 it is seen that a is negative

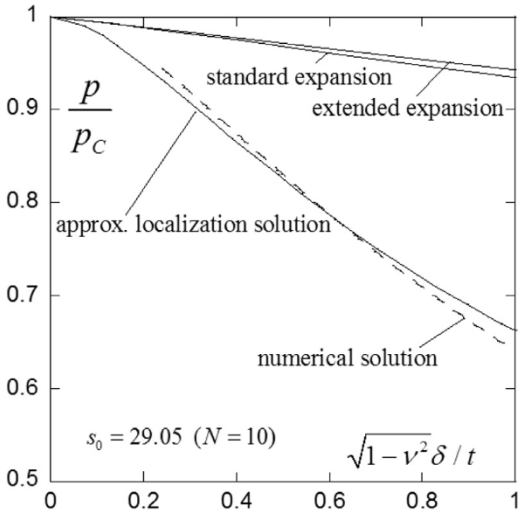

Fig. 4. Axisymmetric post-buckling response of a shallow spherical shell with $s_0 = 29.05$ ($N = 10$) subject to external pressure according to Koiter's standard post-bifurcation expansion (Section 2.3), to Koiter's extended expansion (Section 2.4), to the approximate Rayleigh-Ritz solution (Section 3) and from a direct numerical solution of the shallow shell equations presented in Section 1.3. These dimensionless results are independent of ν. The numerical solution has been included over the range of pressures where it is accurate, i.e., everywhere except in the immediate vicinity of the bifurcation point.

(favoring inward buckling at the pole, since $p < p_c$ corresponds to $(a\xi) < 0$, i.e., $\xi > 0$, i.e., $\tilde{w}(0) \approx \xi w_1(0) < 0$) and relatively small in magnitude compared to b. Further, a approaches zero as the dimensionless cap radius s_0 becomes large. For fixed dimensional quantities, R and $\bar{s}_0$, this implies that $a \approx 0$ for thin shells with small t/R, similar to the findings of Thompson (1964) and Koiter (1969) for the full sphere. This lowest order result suggests weakly unstable buckling behavior with very little tendency to favor inward rather than outward deflections at the pole, which is very much at odds with experimental observations for spherical shells. The failure of the lowest order nonlinear expansion to capture the expected highly unstable buckling behavior drove Koiter to examine the second order terms in the expansion in considerable depth in his 1969 paper. The second order coefficient b in Fig. 3 is negative and significantly larger than a. Furthermore, it approaches a finite value ($b \approx -0.132$) as s_0 becomes large. Nevertheless, the predicted buckling instability is still rather weak, as Koiter also found from his analysis of the full sphere. The plot in Fig. 4, which includes the accurate numerical analysis of the shallow cap (similar to that for the full sphere in the Introduction) and two other results developed later, makes this evident.

Fig. 4 displays curves of p/p_c versus the dimensionless inward buckling deflection at the pole, $\sqrt{1-\nu^2}\delta/t$. Noting that $\sqrt{1-\nu^2}\delta/t = -\tilde{w}(0)/\sqrt{12}$ and $w_1(0) = -J_0(0) = -1$, one finds to second order in ξ

$$\frac{\sqrt{1-\nu^2}\delta}{t} = \frac{1}{\sqrt{12}}(\xi - \xi^2 w_2(0)).$$

This equation together with $p/p_c = 1 + a\xi + b\xi^2$ generates the post-buckling curve for a shell with $s_0 = 29.05$ ($N = 10$) in Fig. 4 labeled as the 'standard expansion'.[1] As Koiter (1969) observed for his analysis of the full sphere, the standard expansion method fails to capture the dramatic loss in post-buckling load carrying capacity. In fact, Koiter argues that the range of validity of the standard expansion for the spherical shell buckling problem goes to zero as $t/R \to 0$.

2.4. Koiter's extended post-buckling expansion

In an attempt to extend the range of validity of the post-buckling expansion, Koiter (1969) modified the standard expansion by evaluating the second order buckling contribution, w_2, at p, not at p_c as in the standard method. His rationale for doing so in the case of the sphere is due to the clustering of eigenmodes at eigen-pressures only slightly above p_c. It turns out that this modification is almost trivially implemented for the present problem. The extended method occupies a substantial section of Koiter's 1969 paper, in part, because he includes the extensive analytical reductions of integrals and sums which are bypassed here with the aid of numerical integration and summation.

Our rendering of the modified expansion of Koiter (1945, 1969) is presented in the Supplementary Materials. The central results for the shallow shell are as follows. The buckling displacement is expanded as

$$\tilde{w}(s) = \xi w_1(s) + \xi^2 w_2(s, p) + \cdots \tag{2.14}$$

[1] The coefficients a and b depend on the normalization of ξ which in turn depends on the way w is rendered dimensionless. It is more common to have $p/p_c = 1 + \hat{a}(\delta/t) + \hat{b}(\delta/t)^2 + \cdots$, see, e.g., Koiter (1969). The two sets of coefficients are related by $\hat{a} = \sqrt{12(1-\nu^2)}a$ and $\hat{b} = 12(1-\nu^2)b$.

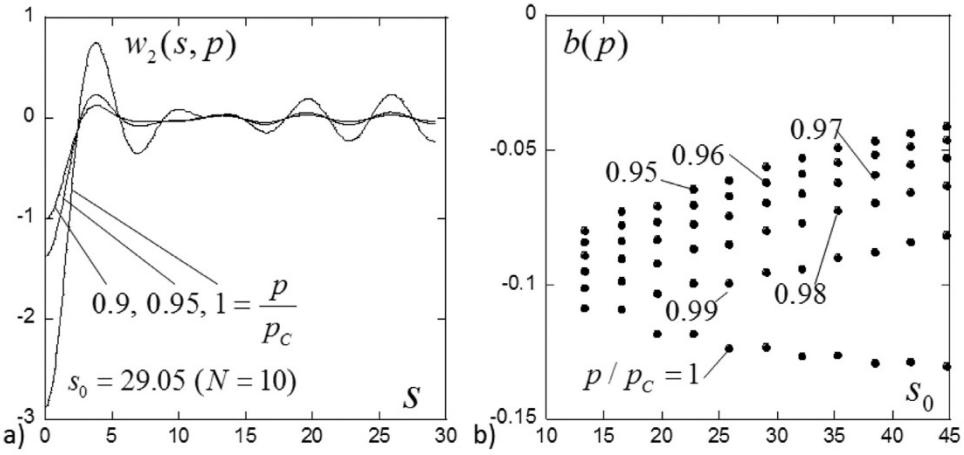

Fig. 5. a) Plots of $w_2(s, p)$ for three values of p/p_c as computed using Koiter's extended method. The curve for $p/p_c = 1$ is the same as that for the standard method. b) Values of $b(p)$ for a range of $s_0 = r_N$, $5 \le N \le 15$, computed with $M = 40$.

where $w_1(s) = -J_0(s)$ is unchanged but w_2 is now evaluated at the current pressure p and not at the bifurcation pressure p_c. The post-buckling expansion then takes the form

$$\frac{p}{p_c} = 1 + a\xi + b(p)\xi^2 + \cdots \tag{2.15}$$

The coefficient a remains unchanged, depending only on w_1 and given by (2.12); the formula for b, given in the Supplementary Materials, also reduces to that for the standard expansion in (2.12) when one accounts for the orthogonality of w_2 to w_1, but b now depends on p due to the presence of w_2.

The boundary value problem for w_2 in the extended method differs slightly from that in (2.9) and writes

$$\nabla^4 w_2 + w_2 + \frac{p}{2}\nabla^2 w_2 = -\frac{p_c}{2} a \nabla^2 w_1 + q_2(s) \tag{2.16}$$

with the same homogeneous boundary conditions and with q_2 as defined earlier. The solution for w_2 is identical to that presented in (2.11a) and (2.11b) except that p_c in the formula for $w_2^{(i)}$ in (2.11b) is replaced by p, i.e.,

$$w_2^{(0)} = q_2^{(0)} \quad w_2^{(N)} = 0 \quad w_2^{(i)} = \frac{1}{(\mu_i^4 + 1 - p\mu_i^2)} q_2^{(i)}, \quad i \ge 1 (\ne N). \tag{2.17}$$

Plots of $w_2(s, p)$ are shown in Fig. 5 for $p/p_c = 1$, 0.95 and 0.9 for a shell with $s_0 = 29.05$ ($N = 10$). The plot for $p/p_c = 1$, which is the same as that for the standard expansion, is not localized to the pole. However, already at $p/p_c = 0.95$, w_2 is nearly localized at the pole. Moreover, the amplitude of w_2 at the pole depends strongly on p/p_c, as does the second order coefficient $b(p)$ which is also plotted in Fig. 5.

The prediction of the pressure function of the pole deflection δ generated by the extended method using (2.15) is included in Fig. 4 for a shell with $s_0 = 29.05$ ($N = 10$). Evidently, while the extended method does capture localization in w_2, it is not successful in extending the range of the of the post-buckling expansion. Indeed, for the case in Fig. 4, the range of the extended method appears to be slightly smaller than that of the standard method. Koiter's application of his extended method (Koiter, 1969) to the full sphere is more successful in extending the range of the expansion but, as he emphasizes, its validity remains severely limited.

3. An approximate localization analysis

In this section, we present an approximate localization analysis of the shallow shell model presented in Section 1.3.

The purpose is twofold. First, it will reveal very clearly why both variants of Koiter's method, the standard one and its extension, have such a small range of validity—the essential reason being that the dominant term in the expansion, $\xi w_1(s)$, does not incorporate localization. Secondly, the approximate method presented in this section captures and clearly reveals the remarkably abrupt nature of the localization behavior. A rigorous analytical expansion that captures localization will be presented Section 4. Here, an approximate Rayleigh-Ritz-type method is employed to analyze the initial post-buckling behavior of the shell.

We use trial functions of the form

$$\tilde{w}(s) = \xi \,\mathrm{sech}(\eta s) w_1(s) + \xi^2 w_2(s, p) \tag{3.1}$$

where ξ and η are the two free parameters which will be varied to render the full energy functional $\Phi(\tilde{w}, p)$ in (2.3) stationary.

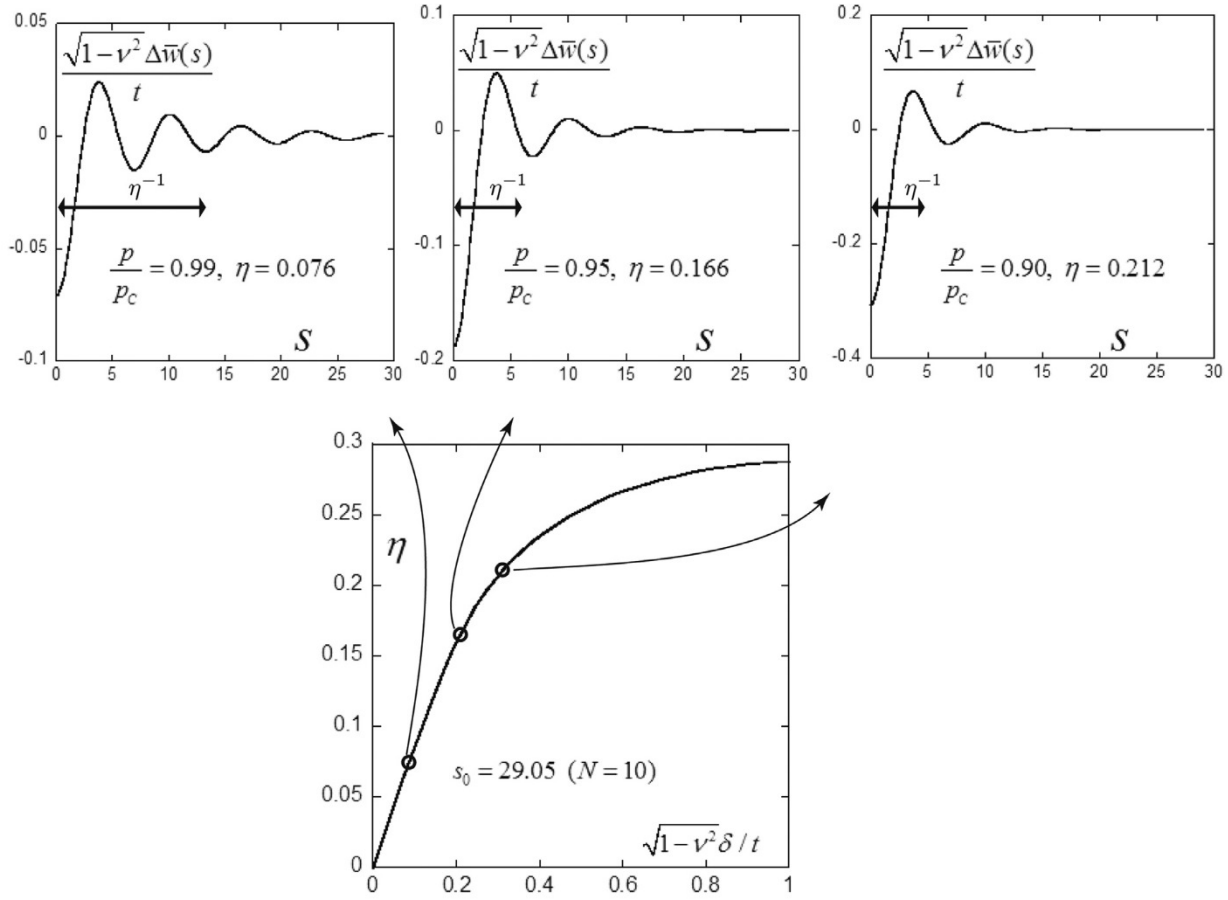

Fig. 6. Predictions of the approximate localization analysis (Section 3) with $s_0 = 29.05$ ($N = 10$). *Top row*: The buckling deflection, $\Delta\bar{w}(s) = \bar{w}(s) - \bar{w}_0$, in dimensionless form at three values of p/p_c displaying the development of localization. *Bottom figure*: The localization parameter, η, as a function of the dimensionless inward pole buckling deflection.

Now, $w_1(s) = -J_0(s)$ continues to be the classical bifurcation mode, and $w_2(s, p)$ is the second order displacement function obtained in the previous section for the extended method. The relatively simple choice (3.1) builds upon the extended solution and brings in a new ingredient: the multiplicative function $\mathrm{sech}(\eta s) = 1/\cosh(\eta s)$ 'turns off' the first order buckling contribution at a tunable distance $\sim 1/\eta$ from the pole. This introduces an adjustable amount of localization. For $\eta = 0$, the exact expansion to second order in ξ is recovered. As has already been noted, $w_2(s, p)$ from the extended analysis reflects localization at values of p below p_c so it has not been modified.

First order terms analogous to $\xi\,\mathrm{sech}(\eta s) w_1(s)$ emerge in rigorous analytical localization analyses such as that of Wadee et al. (1997) who carried out an extensive study of buckling localization of an infinite elastic beam on a nonlinear elastic foundation, a problem with much in common with the spherical shell problem but analytically simpler. Wadee et al. (1997) have illustrated the effectiveness of a Rayleigh-Ritz approach using trial functions suggested by their analytical localization expansion. A first order term qualitatively similar to $\xi\,\mathrm{sech}(\eta s) w_1(s)$ will also emerge in the localization analysis carried out in Section 4, including a prescription for the dependence of η on p. When $\eta = 0$, $\tilde{w}$ in (3.1) satisfies all the boundary conditions. When localization is fully in effect and $\mathrm{sech}(\eta s_0) \approx 0$, $\tilde{w}$ also satisfies all the boundary conditions. There is a small range of η, roughly $0 < \eta < 2/s_0$, wherein the natural boundary conditions at s_0 are only approximately met by the term $\xi\,\mathrm{sech}(\eta s) w_1(s)$, however in the range of interest when localization is in effect, the conditions are met.

The procedure for rendering Φ stationary for any prescribed p can be described as follows. Given the function $\tilde{w}$, $\Phi(\xi, \eta, p)$ in (2.3) is evaluated numerically to high accuracy given a prescribed p for any values of the two free parameters ξ and η. Stationarity requires $\partial\Phi/\partial\xi = 0$ and $\partial\Phi/\partial\eta = 0$. These equations are solved using a Newton iteration method with all derivatives with respect to ξ and η evaluated numerically. The result of this process for a shell with $s_0 = 29.05$ ($N = 10$) is included in Fig. 4 for pressure versus pole buckling deflection. Companion plots of the buckling deflection, $\sqrt{1-\nu^2}\,\Delta\bar{w}(s)/t = \tilde{w}(s)/\sqrt{12}$, and of the localization parameter η as a function of the dimensionless pole buckling deflection are given in Fig. 6.

The relatively simple trial buckling mode in (3.1) coupled with the Rayleigh-Ritz analysis transparently captures buckling localization in the spherical shell subject to external pressure. Moreover, the results in Figs. 4 and 6 clearly reveal why the conventional initial post-bifurcation expansions, including Koiter's extended method, have such a limited range of validity. Note from Fig. 6 that at pole buckling deflections as small as 1/10 of the shell thickness, $\eta \approx 0.1$ such that the mode has already undergone significant localization, i.e., there is a substantial zone around the edge of the shell with $\tilde{w} \approx 0$ and $w \approx w_0$. At pole deflections on the order of 1/2 the shell thickness the mode is essentially fully localized at the pole with $w \approx w_0$ everywhere outside the dimple. The abruptness of the localization is the reason that the standard initial post-bifurcation expansion has such a small range of validity. These results also explain why Koiter's attempt to extend the range of validity by modifying w_2 but not w_1 could only have modest success. The asymptotic post-buckling results obtained by Baumgarten and Kierfeld (2019) also reveal a transition in the response of pressure versus pole deflection associated with localization at the small pole deflections noted above.

The localization analysis presented in this section generates a reasonably accurate approximation to the post-buckling response for inward pole deflections as large as one shell thickness, corresponding to pressures falling to about 60% of the classic buckling pressure. This range could almost certainly be extended with more elaborate trial functions having more free parameters. That extension is not pursued in this paper because of the availability of the accurate numerical solution referred to in the Introduction. The primary objective of this paper is to expose the abrupt nature of the localization process immediately following bifurcation and to provide insights into the analytical form the localization takes by modifying the classical buckling mode. We believe the approximate analysis in this section and the more rigorous localization expansion to follow achieves this objective.

4. An asymptotic solution capturing localization

In this section, we derive a weakly non-linear solution to the shallow shell equations summarized in Section 1.3. We work in the limit $s_0 = \infty$ where the edge is at infinity, implying that we ignore the immediate aftermath of bifurcation where the buckling pattern extends beyond the 'endpoint' s_0. In view of the above numerical results, this assumption is already reasonably for $p/p_c = 0.99$, and highly accurate for $p/p_c = 0.95$. It is possible to extend our results to the case of a finite s_0 but this does not bring much more insight (as discussed in the conclusion) and it is significantly more complicated: it requires handling boundary conditions at the edge s_0. Here, we will simply require that the solutions vanish asymptotically for $s \to \infty$. Our approach complements the recent results of Baumgarten and Kierfeld (2019) by providing an explicit expression for the post-buckled solution $w(s)$.

The critical value of the pressure corresponding to $s_0 = \infty$ is used in this section, namely

$$p_c = 4.$$

4.1. Expansion strategy

The approach inspired by the classical work on localization of elastic buckling modes in *extended structures* (Amazigo et al., 1970; Coman, 2006; Hunt et al., 1993; Potier-Ferry, 1983). Here 'extended structures' refer to structures whose dimensions are much larger than the typical wavelength of their linear bifurcation mode: a shallow shell is an extended structure in this sense, in the limit $s_0 \gg 1$ considered here, see the discussion above Eq. (1.10).

In extended structures, the buckling mode, initially spreading over the entire domain, often localizes in the post-buckling regime. This localization has been described in extended systems such as elastic struts on a nonlinear foundation (Amazigo et al., 1970; Hunt et al., 1993) or on a fluid foundation (Audoly, 2011; Pocivavsek et al., 2008). In these works, the localization has been analyzed by means of a two-scale expansion: the buckling mode is sought in terms of a 'fast' variable s capturing the rapid oscillations already present in the linear buckling mode, as well as a 'slow' variable $x = \xi s$ capturing an amplitude modulation. The connection $x = \xi s$ between the slow and fast variables makes use of the same expansion parameter ξ as that appearing in Koiter's expansions, $|\xi| \ll 1$, representing an arc-length along the bifurcated branch in the bifurcation diagram. In the two-scale expansion, the fast variable s is ultimately averaged out, which leads to so-called *amplitude equations* involving the slow variable only. These amplitude equations can be solved and they capture the localization effectively, as we shall show.

The above is a general strategy to address localization. In the particular case of shallow axisymmetric shells, there is an additional complication: localization takes place at the pole $s = 0$, which happens to be a singular point of the ordinary differential Eqs. (1.14a–1.14b) governing the equilibrium. As a result, the two-scale expansion cannot yield directly the boundary conditions applicable at the pole for the amplitude equations: the amplitude equation brings in divergences at the poles, and boundary layer analysis is required to resolve these divergences. Boundary layer equations need to be derived, which replace the boundary conditions used in simpler extended structures. They play a key role: the nonlinearity that ultimately selects the buckling amplitude arises from the polar layer, as we shall show.

4.2. Expansions

This strategy is carried out by postulating the following expansions.

- The load p is expanded as before in terms of an 'arc-length' parameter ξ, see Eq. (2.8),

$$\frac{p}{p_c} = 1 + a\xi + b\xi^2 + \cdots \tag{4.1}$$

where $p_c = 4$.

- The solution for the tangential and outward normal displacements $u(s)$ and $w(s)$ is sought in the *outer region* ($s \gg 1$) in the form $w_{out}(s) = w_0(s) + \tilde{w}_{out}(s)$ and $u_{out}(s) = u_0(s) + \tilde{u}_{out}(s)$ where $w_0(s)$ and $u_0(s) = 0$ represent the uniform solution, see Eq. (2.1), and the buckling displacements $\tilde{w}_{out}$ and $\tilde{u}_{out}$ are given by a two-scale expansion,

$$\begin{aligned}\tilde{w}_{out}(s) &= \xi^\alpha \Re\left[e^{is}\left(W_{[0]}(x) + \xi W_{[1]}(x) + \frac{\xi^2}{2}W_{[2]}(x) + \cdots\right)\right]\\ \tilde{u}_{out}(s) &= \xi^\alpha \Re\left[e^{is}\left(U_{[0]}(x) + \xi U_{[1]}(x) + \frac{\xi^2}{2}U_{[2]}(x) + \cdots\right)\right]\end{aligned} \tag{4.2}$$

where

$$x = \xi s$$

is the slow variable, $\Re$ represents the real part operator, i is the unit imaginary number $i = \sqrt{-1}$, α is an exponent to be determined later and $W_{[0]}(x)$ and $U_{[0]}(x)$ are complex-valued functions.

- The solution in the polar layer, for $s = \mathcal{O}(1)$, is sought as a regular (single-scale) perturbation in terms of the *slow* variable s,

$$\begin{aligned}\tilde{w}_{in}(s) &= \xi^\beta\left(\check{W}_{[0]}(s) + \xi\check{W}_{[1]}(s) + \frac{\xi^2}{2}\check{W}_{[2]}(s) + \cdots\right)\\ \tilde{u}_{in}(s) &= \xi^\beta\left(\check{U}_{[0]}(s) + \xi\check{U}_{[1]}(s) + \frac{\xi^2}{2}\check{U}_{[2]}(s) + \cdots\right)\end{aligned} \tag{4.3}$$

where β is a second exponent, to be determined later, and $\check{W}_{[0]}(s)$ and $\check{U}_{[0]}(s)$ are real-valued functions.

The exponential term e^{is} in the outer solution accounts for the oscillations seen both in the linear buckling mode and in the numerical post-bifurcated solutions.

The outer amplitudes $W_{[j]}(x)$ and $U_{[j]}(x)$, the inner solutions $\check{W}_{[j]}(s)$ and $\check{U}_{[j]}(s)$, as well as the coefficients a and b and the exponents α and β will be determined by inserting these expansions into the shallow shell equations, and by solving order by order with respect to ξ. As part of the solution process, we will ensure that the outer and inner solutions can be matched in the so-called *intermediate region*, defined as the domain overlapping the inner and outer regions.

4.3. Scaling analysis

Before proceeding to insert the expansions above into the equations of equilibrium, we start by a qualitative scaling analysis.

First, we require that the linear buckling mode, which writes $w_1 = A(\xi)J_0(s)$ in the limit $s_0 \to \infty$ (i.e., by setting $\mu = 1$ in Section 2.2), is consistent with expansions postulated above; here, $A(\xi)$ is the buckling amplitude, which remains unspecified in the linear bifurcation analysis. A large-s expansion of the Bessel function J_0 writes $w_1 = A(\xi)(\frac{\cos s}{\pi\sqrt{s}} + \frac{\sin s}{\pi\sqrt{s}}) + \cdots = [\frac{A(\xi)\sqrt{\xi}}{\pi}]\Re[e^{is}(\frac{1-i}{\sqrt{x}} + \cdots)]$ where the dots denote higher-order terms, of order $s^{-3/2}$. This expression can be identified with the leading-order term in the expansion $\tilde{w}_{out}(s)$ in the outer region $s \gg 1$, see Eq. (4.2), provided we identify $[A(\xi)\sqrt{\xi}] \sim \xi^\alpha$ and $W_{[0]}(x) \sim \frac{1-i}{\pi\sqrt{x}}$. On the other hand, $w_1 = A(\xi)J_0(s)$ can be identified directly with the inner expansion (4.3) with $A(\xi) \sim \xi^\beta$ and $\check{W}_{[0]}(s) \sim J_0(s)$. Eliminating $A(\xi)$ from these two relations, we conclude $\xi^\alpha \sim A(\xi)\sqrt{\xi} \sim \xi^{\beta+1/2}$, which imposes

$$\alpha = \beta + \frac{1}{2}. \tag{4.4}$$

A similar reasoning based on the tangent displacement $u_1(s) = A(\xi)J_1(s)$ of the linear buckling mode leads to the same relation between α and β.

Next, we observe that the only nonlinearity present in the variational formulation (1.11–1.13) of the shallow shell model is the term $\frac{1}{2}w'^2$ found in the strain E_θ. This is thus the nonlinearity that will ultimately enter into the nonlinear equation and will set the buckling amplitude. We know from simulations that the localization takes place at the pole: we assume that the nonlinearity plays a role in the polar (inner) region. There, it can be estimated as $\tilde{w}'^2 \sim \tilde{w}'^2_{in} \sim \xi^{2\beta}$. Next, we try to guess which is the other term with which this nonlinearity is balanced in the equation for the buckling amplitude. If we attempt to balance the nonlinear term with the other, linear terms present in the strain E_θ, namely $w_{in} \sim \xi^\beta$ and $u'_{in} \sim \xi^\beta$, we arrive to $t^{2\beta} \sim t^\beta$, i.e., $2\beta = \beta$; however, this is inconsistent with the requirement $\beta > 0$ warranting that the buckling amplitude goes to zero near threshold (for $\xi \to 0$). As we will see later, this paradox is resolved by balancing the nonlinear

term $\tilde{w}'^2_{\text{in}} \sim \xi^{2\beta}$ with the *subdominant corrections* to the linear terms $\tilde{w}_{\text{in}}$ and $\tilde{u}'_{\text{in}}$ entering in the strain E_θ; both of latter are of order $\sim \xi \times \xi^\beta = \xi^{\beta+1}$. The balance then yields $\xi^{2\beta} = \xi^{\beta+1}$, hence $\beta = 1$. With the help of (4.4), this suggests

$$\alpha = \frac{3}{2} \quad \beta = 1. \tag{4.5}$$

Even though we can offer no mathematical proof, we expect that these particular values are the only ones that can make the asymptotic matching procedure work. In the following, we will use Eq. (4.5) as a starting point to derive the leading order terms in the solution. We will check at the end that the predictions are consistent with the numerical results.

4.4. Main steps of the asymptotic construction

A complete derivation of the asymptotic solution is given in the Supplementary Material. A summary of the main results is presented here.

4.4.1. Regions

The different regions used in the expansion are defined by

$$\begin{cases} \text{inner region:} & s \ll \left(1-\frac{p}{4}\right)^{-1/2} \\ \text{intermediate region:} & 1 \ll s \ll \left(1-\frac{p}{4}\right)^{-1/2} \\ \text{outer region:} & 1 \ll s. \end{cases}$$

Note that the intermediate region is the intersection of the inner (polar) and outer regions.

4.4.2. Outer solution

By inserting the outer expansion in the equations for the shallow shell, we first obtain

$$a = 0, \tag{4.6}$$

which is consistent with the prediction of Koiter's method for $s_0 \to \infty$, see Section 2 and Fig. 3 in particular. In view of (4.1), the relation between the load and the expansion parameter ξ becomes

$$\sqrt{-b}\xi \approx \left(1-\frac{p}{4}\right)^{1/2}. \tag{4.7}$$

By solving the equilibrium equations for the shell order by order, we find the dominant solution in the outer region as $W_{[0]}(x) = \frac{C_1+iC_2}{\sqrt{x}} \exp(-\sqrt{\frac{-b}{2}}x)$, where the real constants of integration C_1 and C_2 and the coefficient b will be determined later by matching with the outer solution. Inserting into (4.2), we find the buckling deflection as

$$\tilde{w}_{\text{out}}(s) = \xi \frac{C_1 \cos s - C_2 \sin s}{\sqrt{s}} \exp\left(-\left[\frac{1}{2}\left(1-\frac{p}{4}\right)\right]^{1/2} s\right) + \cdots \tag{4.8}$$

The coefficient in square bracket in the exponential produces a fast localization in the post-buckling regime, as discussed in Section 4.5.

4.4.3. Inner solution

The inner solution is found similarly by inserting the expansions (4.3) into the equilibrium equations for shallow shells. The result is

$$\begin{aligned} \tilde{W}_{[0]}(s) &= C_3 J_0(s) \\ \tilde{W}_{[1]}(s) &= C_6 J_0(s) + \frac{C_5}{2} s J_1(s) + \left(-C_4 + \frac{C_3^2}{4}\right)\left(1 - J_0(s) - \frac{s}{2}J_1(s)\right) + \frac{\pi}{4} C_3^2\, G(s) \end{aligned}$$

where $G(s)$ is a numerical function defined in terms of Bessel functions, defined in the Supplemental material, and $C_3, \ldots, C_6$ are constants of integration. By contrast with what happened in the outer region, both the dominant order solution $\tilde{W}_{[0]}(s)$ *and the subdominant one* $\tilde{W}_{[1]}(s)$ are required in the inner region for matching, see below.

An expression for $\tilde{w}_{\text{in}}(s)$ is found by inserting the above solution into (4.3).

4.4.4. Matching

By requiring that the inner and outer solutions match in the intermediate region, we find two constants of integration as $C_1 = \frac{C_3}{\sqrt{2\pi}}$ and $C_2 = -\frac{C_3}{\sqrt{2\pi}}$, and we obtain

$$\gamma C_3^2 + \frac{\sqrt{-b}}{\sqrt{2\pi}} C_3 = 0, \tag{4.9}$$

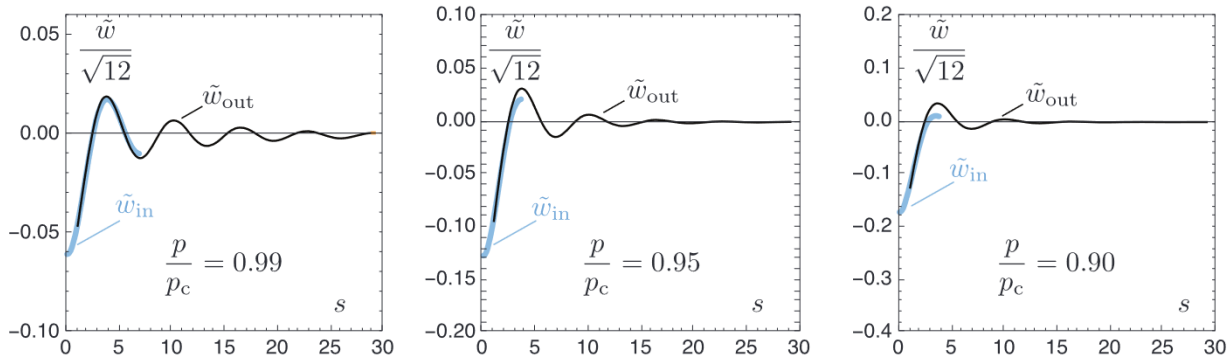

Fig. 7. Progressive localization of the buckling deflection, as predicted by the asymptotic expansion, Eq. (4.11b). Same parameter values and plotting conventions as in Fig. 6. Note the overlap of the inner solution $\tilde{w}_{\text{in}}$ (thicker light blue curve) and the outer solution $\tilde{w}_{\text{out}}$ (thin black curve). (For interpretation of the references to colour in this figure legend, the reader is referred to the web version of this article.)

Here, γ a numerical constant,

$$\gamma = \frac{\sqrt{\pi}}{4}\int_0^\infty \left(\frac{[J_0(u)]^2+[J_1(u)]^2}{4} + \frac{2}{u}J_0'(u)J_0''(u)\right)uJ_0(u)\mathrm{d}u \tag{4.10a}$$

whose value is

$$\gamma = \frac{3\sqrt{3}}{16\sqrt{\pi}} = 0.183\,226. \tag{4.10b}$$

By multiplying both sides of Eq. (4.9) by ξ^2, one makes appear the load p from Eq. (4.7) and the outward normal displacement at the pole $\tilde{w}(0) \approx \xi^{3/2}\bar{W}_{[0]}(0) = \xi^{\beta}C_3J_0(0) = C_3\xi$. This leads to the *bifurcation equation*

$$\left(\tilde{w}(0) + \frac{1}{\gamma\sqrt{2\pi}}\left(1-\frac{p}{4}\right)^{1/2}\right)\tilde{w}(0) = 0.$$

It has two solutions: the unbuckled one $\tilde{w}(0) = 0$, and the buckled one.

4.5. Results

The main predictions of the matched asymptotic theory are as follows. The buckling amplitude at the pole is predicted as

$$\tilde{w}(0) = -\frac{1}{\gamma\sqrt{2\pi}}\left(1-\frac{p}{4}\right)^{1/2}, \tag{4.11a}$$

and the solution for the deflection writes

$$\tilde{w}(s) = \tilde{w}(0) \times \begin{cases} J_0(s) + \left[\frac{1}{2}\left(1-\frac{p}{4}\right)\right]^{1/2} sY_1(s) + \cdots & \text{(inner region)} \\ \frac{\cos\left(s-\frac{\pi}{4}\right)}{\sqrt{\frac{\pi s}{2}}}\exp\left(-\left[\frac{1}{2}\left(1-\frac{p}{4}\right)\right]^{1/2}s\right) + \cdots & \text{(outer region)} \end{cases} \tag{4.11b}$$

Here, Y_1 denotes the Bessel function of the second kind. The matching procedure ensures that the alternatives in the right-hand side above are consistent in the intermediate region: there, both can be approximated as

$$\tilde{w}(s) = \tilde{w}(0)\frac{\cos\left(s-\frac{\pi}{4}\right)}{\sqrt{\frac{\pi s}{2}}}\left(1-\left[\frac{1}{2}\left(1-\frac{p}{4}\right)\right]^{1/2}s + \cdots\right). \quad \text{(intermediate region).} \tag{4.11c}$$

Note that the expansion parameter ξ has been eliminated from this final set of results.

Eq. (4.11a) predicts that the deflection is inward at the pole, in accord with the experimental and numerical observations.

The deflection predicted by Eq. (4.11b) is plotted in Fig. 7 for different values of the pressure. The exponential in the outer solution produces a fast localization: due to the coefficient appearing in the square bracket, the amplitude of the oscillations is reduced significantly at a distance of order $s \sim [\frac{1}{2}(1-\frac{p}{4})]^{-1/2}$ from the pole. This yields the following estimate for the number n_{osc} of oscillations where the cut-off takes place,

$$n_{\text{osc}} = \left[\frac{1}{2}\left(1-\frac{p}{4}\right)\right]^{-1/2} \Big/ (2\pi). \tag{4.12}$$

The set of plots in Fig. 7 (asymptotic method) and in Fig. 6 (approximate method) were produced using the same set of values of the loading $\frac{p}{4} = \{0.99, 0.95, 0.90\}$. They show very similar results—the two figures do not exactly agree, however,

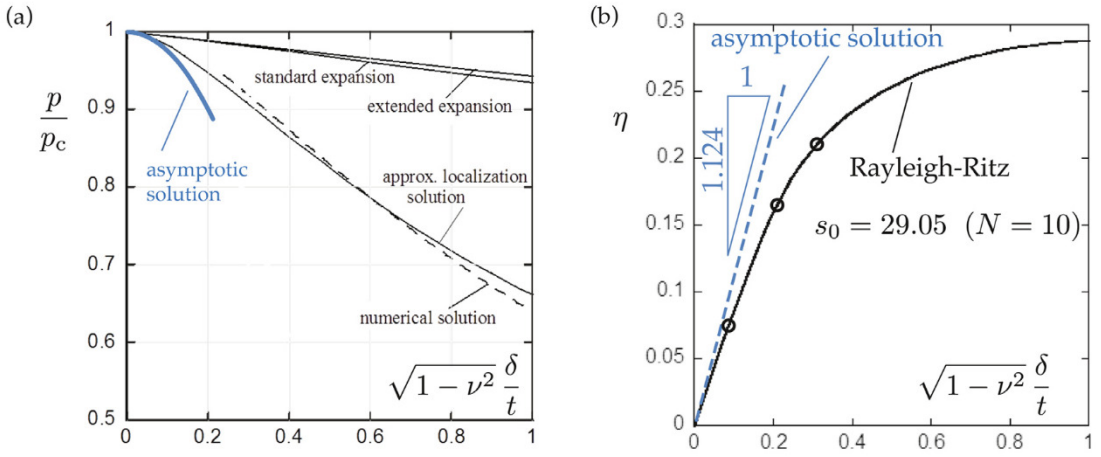

Fig. 8. (a) Bifurcation curves showing the deflection at the pole scaled by the thickness versus the dimensionless pressure, as predicted by the different models; same data as in Fig. 4 except for the new curve corresponding to the asymptotic solution (thick blue curve). (b) Comparison of the inverse localization length (vertical axis) versus the scaled deflection at the pole for the asymptotic and approximate localization analyses. (For interpretation of the references to colour in this figure legend, the reader is referred to the web version of this article.)

as the ansatz in Eq. (3.1) is not asymptotically exact. The above formula yields estimates $n_{\rm osc} = \{2.3, 1.0, 0.7\}$ for these respective values of $\frac{p}{4}$. This captures how the number of bumps seen in both sets of figures evolves with p. When the pressure is only 1% less than the critical pressure, $\frac{p}{4} = 0.99$ (first plot), the estimated residual number of bumps, $n_{\rm osc} = 2.3$, is already quite small: the asymptotic solution captures the quick localization. For $\frac{p}{4} = 0.95$, the predicted number of oscillations is so small, $n_{\rm osc} = 1.0$, that the main assumption of the matched asymptotic theory, namely a clear separation between the scale $s \sim 1$ of the oscillations and the scale $s \sim (1 - \frac{p}{4})^{-1/4}$, is no longer satisfied: the asymptotic theory cannot yield accurate results for $p/4$ less than ~ 0.95. In accord with this, the overlap between the outer and inner solutions becomes limited below $\frac{p}{4} \sim 0.95$.

An estimate of the pressure $p_{\rm flat}$ where the curvature at the pole becomes zero, *i.e.*, when the outward curvature brought about by buckling balances the initial inward curvature, can be obtained by solving $\tilde{w}''_{\rm in}(0) = -\frac{1}{\sqrt{12(1-\nu^2)}}$. Using the expression of $\tilde{w}_{\rm in}$ in Eq. (4.11b), we can solve this equation as $\frac{p_{\rm flat}}{4} = 1 - (\frac{2\gamma\sqrt{2\pi}}{\sqrt{12(1-\nu^2)}})^2 = 0.923$ (with $\nu = 0.3$). This pressure is too small for the asymptotic theory to be accurate, but this suffices to confirm that the buckling is already fully localized by the time the curvature at the pole changes sign, as discussed in Section 1.1.

The inward deflection at the pole scaled by the thickness writes, in our units,

$$\sqrt{1-\nu^2}\frac{\delta}{t} = -\frac{\tilde{w}_{\rm in}(0)}{\sqrt{12}} = \frac{1}{\gamma\sqrt{24\pi}}\left(1-\frac{p}{4}\right)^{1/2} = \frac{8}{9\sqrt{2}}\left(1-\frac{p}{4}\right)^{1/2}, \tag{4.13}$$

and we recover the result obtained by Baumgarten and Kierfeld (2019) by a direct method. In Fig. 8(a), this prediction is compared to the predictions of the other models. The range of pressure where the asymptotic theory roughly agrees with the approximate Rayleigh-Ritz solution is limited, but consistent with the estimate $1 \le \frac{p}{4} \lesssim 0.95$ warranting scale separation.

A more detailed comparison of the asymptotic and approximate localization analyses can be made by identifying the localizing terms $\mathrm{sech}(\eta s)$ in (3.1) and $\exp(-[\frac{1}{2}(1-\frac{p}{4})]^{1/2}s)$ in Eq. (4.11b). Using the equivalent $\mathrm{sech}(\eta s) \propto \exp(-\eta s)$ for large s, this suggests $\eta \equiv [\frac{1}{2}(1-\frac{p}{4})]^{1/2} = \frac{1}{0.629\sqrt{2}} \times \sqrt{1-\nu^2}\frac{\delta}{t} = 1.124(\sqrt{1-\nu^2}\frac{\delta}{t})$. This is the dashed blue prediction shown in Fig. 8(b). The agreement is good up to deflections of the order one tenth of the thickness, which is in line with the domain of validity of the asymptotic theory. Note that the asymptotic and approximate localization analyses are not equivalent to one another, even for small buckling amplitudes: this is why the slope of the dashed blue curve in Fig. 8(b) does not exactly match the initial tangent to the full curve; the slopes still agree within about 20%.

5. Discussion and conclusion

In this paper, we have analyzed the localization of buckling in spherical shells based on the shallow shell model. If we had instead used a full (i.e., non-shallow, geometrically exact) shell model, we would have obtained (slightly) different predictions close to the bifurcation threshold, when the post-buckled solution makes significant oscillations far from the pole. When localization proceeds, however, the oscillations become limited to the neighborhood of the poles, and the shallow shell model produces equivalent predictions as full shell models. Quantitatively, this equivalence holds when the size of the localized region is typically less than, say, half the radius of the shell: in our dimensionless units, this happens when $[\frac{1}{2}(1-\frac{p}{p_c})]^{-1/2} \ll \frac{\frac{1}{2}R}{\sqrt{Rt}/12^{1/4}}$, i.e., $\frac{p}{p_c} \lesssim 1 - 2\frac{2^2}{(R/t)12^{1/2}}$. For the full shell shown in Fig. 1 having an aspect ratio $R/t = 103$, this

yields $\frac{p}{p_c} \lesssim 0.978$ which is very close to 1. Only in the immediate aftermath of the bifurcation, for $1 \lesssim \frac{p}{p_c} \leq 0.978$, does the bifurcated solution depend on the details of the shell model and on the equatorial boundary conditions. As soon as the pressure becomes less, the shallow shell model provides an accurate description. This equivalence of the different shell models has been reported in the simulations, as summarized in the Introduction; the localization analysis done in this paper provides explicit ranges of pressure where the shallow shell model is a good approximation.

Koiter argued that the domain of validity of his expansions goes to zero as the shell's aspect ratio R/t becomes large. This domain of validity can be quantitatively assessed as follows. For Koiter's expansions to be applicable, the post-buckled solution should bear strong resemblance with the linear buckling mode. This requires that the localizing exponential in (4.11b) varies little over the entire domain. For instance, the condition $[\frac{1}{2}(1-\frac{p}{p_c})]^{-1/2} > \frac{5R}{\sqrt{Rt}/12^{1/4}}$ warrants that the localizing exponential varies by at most $1-e^{-1/5}=20\%$ from pole to equator; for a shell with an aspect ratio $R/t=103$ as earlier, this shows that Koiter's expansion breaks down when the scaled pressure becomes less than $\frac{p}{p_c}=1-2\frac{1}{(R/t)5^2 12^{1/2}}=0.9998$.

The characteristic wavelengths of the buckles of a spherical shell subject to external pressure are short compared to the radius of the shell, and the overall pressure carrying capacity attains a maximum when the shell undergoes buckling. These are the two essential elements giving rise to buckling localization wherein the classical buckling mode which covers the entire shell rather abruptly transitions to a localized mode. The qualitative aspects of the phenomenon are similar to those put forward by Considère (1885) for necking localization in long bars stretched in tension. For the perfect spherical shell, the localization process begins at bifurcation in the form of the classical buckling mode modulated by a localizer function which is unity at bifurcation but which begins to alter the shape of the classical buckling mode immediately upon bifurcation. The abrupt alteration of the classical buckling mode is captured by an exact asymptotic localization expansion given in Section 4 and by the approximate Rayleigh-Ritz analysis in Section 3. The approximate Rayleigh-Ritz analysis has the advantage that it provides a good approximation to much larger buckling deflections than the exact asymptotic expansion. In this sense, the spherical shell problem investigated in this paper has much in common with the problem of the buckling of a compressed beam on a nonlinear elastic foundation analyzed in depth using both methods by Wadee et al. (1997). In the Introduction, we have noted that there has been recent progress in exploring localization in the iconic shell buckling problem, the cylindrical shell under axial compression, by Horák et al. (2006), Kreilos and Schneider (2017) and Groh and Pirrera (2019). These authors have exploited new numerical techniques for partial differential equations in their studies. The subject of localization phenomena is ripe for developing new analytical and numerical methods.

The spherical shells in this paper have been taken to be perfect and the recent work on localization in cylindrical shells alluded to above has also been limited to perfect shells. To obtain a full understanding of shell buckling and, in particular, to obtain quantitative estimates of load carrying capacities under realistic conditions, it will be necessary for imperfections to be taken into account. Imperfections, such as initial distortions from the perfect geometry of the shell in the form of a local dimple, can trigger a buckling response that is localized from the start. Localized dimple-like imperfections are generally regarded as more realistic than geometric imperfections assumed to have the shape of a classical buckling mode which extends in a highly coordinated manner over the entire shell. An extensive experimental and numerical study of the buckling of spherical shells with isolated geometric dimple imperfections has been recently published (Lee et al., 2016) which reveals buckling dominated by localized behavior, and the analysis of Baumgarten and Kierfeld (2019) considers the influence of local dimple imperfections.

Supplementary material

Supplementary material associated with this article can be found, in the online version, at doi:10.1016/j.jmps.2019.103720.

References

Amazigo, J.C., Budiansky, B., Carrier, G.F., 1970. Asymptotic analyses of the buckling of imperfect columns on nonlinear elastic foundations. Int. J. Solids Struct. 6 (10), 1341–1356.
Audoly, B., 2011. Localized buckling of a floating Elastica. Phys. Rev. E 84 (1), 011605.
Bauer, L., Reiss, E.L., Keller, H.B., 1970. Axisymmetric buckling of hollow spheres and hemispheres. Commun. Pure Appl. Math. 23 (4), 529–568.
Baumgarten, L., Kierfeld, J., 2019. Shallow shell theory of the buckling energy barrier: from the Pogorelov state to softening and imperfection sensitivity close to the buckling pressure. Phys. Rev. E 99, 022803.
Bushnell, D., 1965. Some Problems in the Theory of Thin Shells Ph.D. dissertation. Stanford University, Stanford, CA, USA.
Coman, C.D., 2006. Inhomogeneities and localised buckling patterns. IMA-J. Appl. Math. 71, 133–152.
Considère, A., 1885. Mémoire sur l'emploi du fer et de l'acier dans les constructions. Annales des Ponts et Chaussées, Série 6 9, 574–775.
Evkin, A., Kolesnikov, M., Prikazchikov, D.A., 2016. Buckling of a spherical shell under external pressure and inward concentrated load: asymptotic solution. Math. Mech. Solids 1–13.
Groh, R.M.J., Pirrera, A., 2019. On the role of localizations in buckling of axially compressed cylinders. Proc. R. Soc. A 475 (2224), 20190006.
Horák, J., Lord, G.J., Peletier, M., 2006. Cylinder buckling: the mountain pass as an organizing center. SIAM J. Applied. Math. 66 (5), 1793–1824.
Hunt, G.W., Wadee, M.K., Shiacolas, N., 1993. Localized elasticae for the strut on the linear foundation. J. Appl. Mech. 60, 1033–1038.
Hutchinson, J.W., 2016. Buckling of spherical shells revisited. Proc. R. Soc. A 472, 20160577.
Hutchinson, J.W., Thompson, J.M.T., 2017. Nonlinear buckling behavior of spherical shells: barriers and symmetry-breaking dimples. Phils. Trans. R. Soc. A 375, 20160154.
von Kármán, T., Tsien, H.-S., 1939. The buckling of thin cylindrical shells by external pressure. J. Aeronaut. Sci. 7 (2), 43–50.
Koiter, W.T., 1945. On the Stability of an Elastic Equilibrium Ph.D. thesis. Technische Hooge School Delft.

Koiter, W.T., 1969. The nonlinear buckling problem of a complete spherical shell under uniform external pressure. Proceedings of the Koninklijke Nederlandse Akademie van Wetenschappen, Series B 72, 40–123.
Kreilos, T., Schneider, T.M., 2017. Fully localized post-buckling states of cylindrical shells under axial compression. Proc. R. Soc. A 473 (2205), 20170177.
Kyriakides, S., Corona, E., 2007. Mechanics of Offshore Pipelines, 1 (Buckling and collapse). Elsevier Science, Oxford, UK.
Lee, A., López Jiménez, F., Marthelot, J., Hutchinson, J.W., Reis, P.M., 2016. The geometric role of precisely engineered imperfections on the critical buckling load of spherical elastic shells. ASME J. Appl. Mech. 83, 111005.
Pocivavsek, L., Dellsy, R., Kern, A., Johnson, S., Lin, B., Lee, K.Y.C., Cerda, E., 2008. Stress and fold localization in thin elastic membranes. Science 320 (5878), 912–916.
Potier-Ferry, M., 1983. Amplitude modulation, phase modulation and localization of buckling patterns. In: Thompson, J.M.T., Hunt, G.W. (Eds.), Collapse: The Buckling of Structures in Theory and Practice. Cambridge University Press, pp. 149–159.
Riks, E., 1970. A Translation of the Stability of Elastic Equilibrium by Warner Tjardus Koiter. Technical Report AFFDL-TR-70-25. Air Force Flight Dynamics Laboratory.
Thompson, J.M.T., 1964. The rotationally-symmetric branching behavior of a complete spherical shell. Proceedings of the Koninklijke Nederlandse Akademie van Wetenschappen, Series B 67, 295–311.
Tvergaard, B., Needleman, A., 1980. On the localization of buckling patterns. J. Appl. Mech. 47 (3), 613–619.
Visual Numerics, Inc., U., 1994. IMSL numerical analysis software.
Wadee, M.K., Hunt, G.W., Whiting, A.I.M., 1997. Asymptotic and Rayleigh-Ritz routes to localized buckling solutions in an elastic instability problem. Proc. R. Soc. A 453, 2085–2107.